van Haren, H. & Puig, P. (2017). Internal wave turbulence in the Llobregat prodelta (NW Mediterranean) under stratified conditions: A mechanism for sediment waves generation? *Marine Geology*, 388, 1-11

Published version: https://dx.doi.org/10.1016/j.margeo.2017.04.008

Link NIOZ Repository: www.vliz.be/imis?module=ref&refid=286619

Internal wave turbulence in the Llobregat prodelta (NW Mediterranean) under stratified conditions: a mechanism for sediment waves generation?

by Hans van Haren[1*], Pere Puig[2]

[1]Royal Netherlands Institute for Sea Research (NIOZ), P.O. Box 59, 1790 AB Den Burg,
the Netherlands.
*e-mail: hans.van.haren@nioz.nl
[2]Institut de Ciències del Mar, ICM-CSIC. Pg. Marítim de la Barceloneta 37-49,
E-408003 Barcelona, Spain.

Abstract

An array of 76 high-resolution temperature sensors at 0.5 m intervals between 5 and 42.5 m off the bottom was moored near the Barcelona harbor buoy in 81 m water depth, between October 2013 and April 2014. The mooring was located just seaward of an extensive sediment wave area developed in the Llobregat River prodelta, with 1 m high crests parallel to the coast and 50-100 m wavelengths. In the NW-Mediterranean, the thermal stratification reaches its maximum penetration through the water column in autumn until it is broken by winter convection. Such a deep stratification affects large-scale sub-inertial slope currents, which are mostly confined to the upper half of the water column, by the hampered vertical exchange of frictional turbulence, and supports near-bottom internal waves between the inertial and buoyancy frequencies. Observed onshelf propagating frontal bores most likely interact with the sediment waves and contribute to their generation, as they are trailed by considerable shear-induced turbulence and high-frequency internal waves close to the buoyancy frequency that have wavelengths matching those of the sediment waves. The bores are either driven by near-inertial or 3-7 day periodic sub-inertial motions just following a brief period of large convective instability at the end of the offshelf flow phase.

1. Introduction

Fine-grained sediment wave fields are ubiquitous seafloor morphological features on continental margins that are commonly observed in prodeltaic environments (e.g., Trincardi and Normark, 1988; Correggiari et al., 2001; Berndt et al., 2006; Fernández-Salas et al., 2007; Urgeles et al., 2007), continental slopes (Faugères et al., 2002;

Verdicchio and Trincardi, 2006; Ribó et al., 2016a,b) and continental rises (see review in Wynn and Stow, 2002). Initially, most of these sediment waves, particularly the ones found on sloping regions, were interpreted as sliding structures. At present, some consensus is forming (see Lee et al., 2002; Urgeles et al., 2011) to consider them as bedforms (rhythmic features generated by the interaction of the fluid and sediment) via bottom (contour) or turbidity currents (Wynn and Stow, 2002), hyperpycnal currents (e.g., Lee et al., 2002; Lobo et al., 2014) or internal waves (e.g., Flood, 1988; Puig et al., 2007; Ribó et al., 2016a,b).

As suggested previously (Hosegood et al., 2004; Bourgault et al., 2014), shoaling and breaking of internal waves and their induced on- and offshelf currents can be an effective transport mechanism of sediment dispersal and may contribute to the shaping of the sedimentary structures. Internal wave breaking follows from nonlinear deformation of the initially sinusoidal (linear) wave-shape in the interior into an S- or Z-shape, thereby creating an onshelf moving turbulent bore (Vlasenko and Hutter, 2002; Klymak and Moum, 2003; Venayagamoorthy and Fringer, 2012). Such bores can generate 60% of the turbulence during a tidal cycle, as has been observed using high-resolution temperature sensors above Great Meteor Seamount (van Haren and Gostiaux, 2012). They are trailed by a sequence of high-frequency internal waves near the buoyancy frequency that have typical wavelengths O(10-100) m.

In the water phase in the NW Mediterranean Sea, (internal) tides are weak and the main internal wave source is at near-inertial frequencies from geostrophic adjustment following the passage of (atmospheric) disturbances. In the NW-Mediterranean, near-inertial motions associated with wind events are the dominant fluctuations over the shelf and slope (Millot and Crépon, 1981; Font et al., 1990; Puig et al., 2001). An observational study by Puig et al. (2007) in the Adriatic Sea suggested that internal waves can play a role in resuspending and transporting sediment in prodeltaic undulated areas. In that study, near-inertial internal waves induced by local wind pulses tend to propagate across the water column through isopycnals and concentrate their energy at the shelf regions where the seasonal thermocline intersects with the seabed, which turns out to be the depth range characterized by having an undulated seafloor (Puig et al., 2007).

Over the Catalan continental margin, a southwestward flow associated to the Northern Current (Millot, 1999) has been described (Salat et al., 1992). A seasonal along-shelf circulation pattern is described for the Barcelona shelf (Grifoll et al., 2013). The summer period is characterized by strong stratification of the water column and significant vertical shear. Fall is dominated by typical easterly storms resulting in a predominant along-shelf force balance between wind stress and pressure gradient. In winter there is weak stratification and vertical velocity profiles are near-homogeneous, due to cooling and low river discharge, which allow the increased wind energy to mix the entire water column. Spring is characterized by highly variable winds and vertical shear and stratification develops due to river discharge and the gradually increasing heat flux.

In this area, the foreset region of the Llobregat River prodelta clinoform exhibits a series of undulations that were initially attributed to sediment creep (Checa et al., 1988). A detailed morphologic and seismo-stratigraphic analysis of these sediment undulations by Urgelés et al. (2007) revealed that they are developed between 35 and 90 m water depth and appear as a series of slightly sinuous crests and swales with an intricate pattern of bifurcating and truncated ridges (Fig. 1). These undulations have up to 1.3 m high crests and 50-100 m wavelengths, decreasing both in amplitude and wavelength with water depth, and are distributed along isobaths parallel to the coast, showing a large lateral continuity up to 2 km (Urgelés et al., 2007). Based on their internal structure and characteristics, these authors identified such undulations as up-slope migrating sediment waves likely generated from hyperpycnal plumes derived from the Llobregat River, although it was pointed out that the overall shape of the sediment wave field suggested a certain control by bottom currents. A subsequent analysis of the Llobregat prodelta sediment waves, together with similar wave field examples found in other Mediterranean prodeltaic deposits (see review by Urgeles et al., 2011) highlighted the potential role of internal waves as the mechanisms responsible for their formation and maintenance. However, the specific interactions of internal waves with sediment waves, for this particular case and elsewhere, are still not well understood (van Haren, 2017).

In order to improve our knowledge on this topic, we designed an instrumented mooring to determine whether mechanisms induced by 'internal waves' supported by the stable vertical density stratification in the water column can generate hydrodynamic structures responsible for and, perhaps, comparable with the morphology of the sediment waves that exist in the Llobregat prodelta. These structures may be able to influence under particular conditions the resuspension - sedimentation of particles near the bottom with a wave length compatible with that of the sediment waves (e.g., Alexander et al., 2001).

In the present study, we focus on the characteristics of internal wave-induced turbulence in the lower half of the water column, between 5 and about 40 m above the bottom, during the autumn-spring variation of stratification. This choice almost covered the depth range of the sediment waves, but was otherwise logistically motivated to minimize wintertime storm impact and shipping hazards. We analyze an array of 1-Hz sampled high-resolution low-noise-level temperature sensors moored just next to the Barcelona harbor pilot buoy (Fig. 1). Although the focus is on wave motions, flows and turbulence in the water phase, we are motivated by the possible effects of the full range of internal waves, from near-inertial frequencies to near-buoyancy frequencies, on the development of the Llobregat prodelta sediment waves.

2. Materials and methods

A total of 76 'NIOZ4' self-contained temperature (T) sensors sampling at a rate of 1 Hz, with precision better than 5×10^{-4}°C and a noise level of about 6×10^{-5}°C (see van Haren et al., 2009, for the predecessor 'NIOZ3' with similar characteristics), were mounted at 0.5 m vertical intervals on a nylon-coated steel cable. Every 4 hours all sensors were synchronized to a standard clock, so that their times were <0.02 s off. The lowest sensor was 5 m from the bottom due to the anchor chain and acoustic releases below the T-sensor array. Three sensors showed calibration problems and two stopped approximately halfway the recording period. These sensors were randomly distributed over the range of sensors. Missing sensor data are linearly interpolated, which has slight, <5%, low-bias impact on turbulence estimates (see below), as was established from previous data by van Haren and Gostiaux (2012). About 3 m above the upper sensor a downward facing 300 kHz acoustic Doppler current profiler (ADCP) was mounted sampling currents and acoustic echo intensity at a rate of once per 300 s, in 1 m vertical intervals (bins). In contrast with optical backscatter observations, 300 kHz echo intensity is sensitive to particles of the size of one mm and larger. Such particles may be large colloids or flocs, but mainly zooplankton and fish and not fine sediment. In fact, the periodic strong upward and downward motions caused by plankton dynamics is a common observation in acoustic reflection signals (e.g., Flagg and Smith, 1989; Plueddemann and Pinkel, 1989), also in the Mediterranean (van Haren, 2014). Because of the 20° slant angle to the vertical of the four acoustic beams and the first sidelobe reflecting off the bottom, the lowest bin with good data was at 3 m from the bottom. The beam spread caused current estimates to be averages over horizontal distances of 2-30 m, depending on the range from the instrument. Thus, currents of horizontal scales O(10 m) or larger are resolved, whereas the much faster sampling T-sensors resolve 0.5 m vertical scales and <0.01 m horizontally. The horizontal current vector components are rotated to along-shelf (v) and cross-shelf (u) directions according to isobaths (Fig. 1).

The instrumented line was moored at 41° 17′N, 2° 11′E, 81 m water depth just seaward of an extensive field of sediment waves (Fig. 1; characteristics in Urgeles et al., 2007) on 18 October 2013 (yearday 290) and recovered on 06 April 2014 (yearday 460). The average local bottom slope is much steeper (10-15º) than the near-inertial internal wave slope $\alpha(1.02f) \approx 1^{o}$: it is thus supercritical for near-inertial internal waves. As pure inertial waves at wave frequency exactly equal to f have zero slope in well-stratified waters, and exist in theory only, the above slope is computed for the main peak-frequency of freely propagating near-inertial waves. The relatively heavy buoyancy element above the instruments assured mooring deflections of <0.2 m in the vertical under current speeds of up to 0.6 m s^{-1}, as was verified from pressure and tilt sensor information.

After correction for slight compressibility and drift effects by subtracting constant values to adjust to a smooth statically stable mean profile for a period of typically 4 days but at least exceeding the inertial period, the T-data are converted into ‘Conservative’ (~potential) Temperature data Θ (IOC, SCOR, IAPSO, 2010). They are used as tracer for density anomaly (σ_θ) variations following the relation $\delta\sigma_\theta = \alpha\delta\Theta$, $\alpha = -0.26\pm0.02$ kg m^{-3} °C^{-1}, where α denotes the apparent thermal expansion coefficient under local conditions. This relation includes the effects of salinity on density variations and has been established from nearby shipborne Conductivity-Temperature-Depth 'CTD' profile data in autumn (Fig. 2). Salinity ('S') intrusions disturbing this relationship sometimes occur in the second half of the record when the stratification is rather weak following the convection in winter. They are recognizable as 'apparent overturns' lasting longer than the mean buoyancy period T_N in detailed computations over short data sections of a few days. Turbulent overturns cannot last longer than T_N and apparent overturns are thus to be excluded from turbulence estimates. On the other hand, in these weakly stratified periods α tends to be larger-negative (Fig. 2c), so that the above more precise estimate can be considered as a conservative one, as turbulent estimates tend to be biased low for the winter period.

The number of T-sensors and their spacing of 0.5 m, in combination with their low noise level, allows for the quantification of turbulence by estimating parameters like dissipation rate ε and vertical eddy diffusivity K_z via the reordering of unstable overturns making every 1-Hz sampled 'density-'(temperature-)profile a static stable one (Thorpe, 1977). This method was originally developed for shipborne CTD-observations in a freshwater lake. In the ocean, however, CTD-observations suffer from mechanical errors imposed by the ship's motions due to surface waves that are communicated through the cable (e.g., Gargett and Gardner, 2008). Such errors, and sensor mismatch errors, do not occur in moored T-sensor data. For details of the method for moored thermistor sensor data, see van Haren and Gostiaux (2012). In the following, averaging over time is denoted by [...], averaging over depth-range by <...>. The specific averaging periods and ranges are indicated with the mean values.

In the next section, time-depth plots will be presented of the Conservative Temperature and of its derived quantity the buoyancy frequency $N = (-g/\rho d\sigma_\theta/dz)^{1/2}$, where $g = 9.81$ m s^{-2} denotes the acceleration of gravity and $\rho = 1026$ kg m^{-3} a reference density, as a measure for stable stratification. Time series will be presented of turbulence dissipation rate averaged over the entire range of temperature sensors. From the ADCP-data, time-depth plots will be presented of both horizontal current components, describing the entire 2D horizontal flow, and the vertical one (w), the echo amplitude I relative to the time mean to remove water attenuation effects and its derived quantity $|\mathbf{S}| = ((du/dz)^2 + (dv/dz)^2)^{1/2}$, the magnitude of destabilizing shear. The latter derived quantity is used to compute the bulk gradient Richardson number $Ri = N^2/|\mathbf{S}|^2$ (Turner, 1979), a measure for the relative importance of stable stratification and destabilizing shear. When Ri becomes smaller than unity, marginal stability may evidence nonlinear perturbations of a parallel shear flow in a three-dimensional stratified fluid (Abarbanel et al., 1984). Here, we assume this is mainly imposed by internal wave breaking causing (shear-induced) turbulent overturning.

3. Observations

a. Overview

Hydrography: In the fall, the deeper waters off the coast of Barcelona are well stratified, predominantly by temperature variations (Fig. 2a) with salinity marginal positively contributing to density variations (Fig. 2b). In winter until early spring, the stratification is strongly reduced by vertical convection, due to cooling near the surface. Then, salinity and temperature contribute about equally to density variations. This implies that small variations in T- and S-properties, advected by the horizontal currents, may cause fluctuations in the relative contributions to density variations with time. Thus during (late) winter, the high-resolution moored T-observations may occasionally show inversions that are partially compensated by salinity to unknown extent. Such inversions potentially create artificial turbulence parameter values. This is indeed observed in the overall depth-time series of the moored observations with a single temperature sensor drift correction for the entire mooring period that is not specifically tuned for detailed (smaller) periods (Fig. 3). For example, the high $<\varepsilon>$-values (Fig. 3g) occurring between days 395 and 410 are unrealistic also because they are maintained for several days. This is despite the naturally larger turbulence dissipation rate estimated in winter and resulting in near-homogeneous waters, compared with stratified autumn conditions in the first month of observations.

The mooring-data overview shows that in the first week after deployment in mid-autumn, the relatively warm near-surface waters are pushed downward (Fig. 3a), while mixing with deeper waters until near-homogeneous winter conditions are reached around day 335 (early December). With the major transition between days 300 and 335 from 'summer-strong' to 'winter-weak' stratified conditions, transitions are observed in other variables as well. In particular, during days 320-323 a major storm event with winds blowing from the East affected the study area (Fig. 4a), with sustained significant wave heights >3 m (not shown) that presumably helped to homogenize the water column down to 80 m water depth.

Currents: Along-shelf currents (Fig. 3b) have an overall mean value of -0.1 m s^{-1} (directed southwestward) with occasionally strong flows reaching -0.6 m s^{-1}. They are observed to be regularly only above the layer of strong stratification, e.g. around day 300 and three times between days 315 and 325, with weaker amplitude flows below and after day 335. A variable dominant sub-inertial periodicity is observed of 3-7 days, see also the kinetic energy spectrum in Fig. 4b. This flow is partially wind-driven, but mainly indirectly via density fronts, as a direct correspondence with local winds is lacking (Fig. 4b). The cross-shelf currents (Fig. 3c) are relatively weaker than the along-shelf currents and have a near-zero mean (<0.01 m s^{-1}), but their amplitudes increase with decreasing stratification, especially near the bottom. Inertial periodicities are observed in the time series of the horizontal current components, but irregularly only and spectra show a rather broad inertial band rather than a peak in kinetic energy (Fig. 4b). With the horizontal current components, the vertical currents (Fig. 3d) transit around day 325 from predominantly downward above the main stratification, to near-bottom upward when the stratification becomes weaker. This transition is not related to a particular local wind event (Fig. 4a). The periodic strong upward (and downward, not visible) motions after day 425 are dominated by diurnal, probably plankton, motions.

Derived variables: As previously mentioned, the stratification of the water column gradually weakened from the autumn to the winter (Fig. 3a). At the beginning of the mooring period, there were three episodes about 15 days apart in autumn, during which the seasonal stratification reaches deep towards the bottom, lifts up again and deepens. This variation is related to a meandering of the near-coastal flow, presumably also affected by the meandering of the Northern Current. Between days 335 (early December) and about 430 (early March), stratification is rather weak and alternates between near-homogeneous stable and, for periods shorter than the buoyancy period, convectively unstable. After day 430, the near-surface spring stable stratification episodically spreads its influence towards the lower half of the water column. With the stable stratification, the destabilizing shear varies from relatively strong in autumn to weak (below noise level) in winter (not shown).

In winter, short periods with enhanced shear are observed in the lower 5 m of the ADCP-range, mainly between days 340 and 420. This shear may be associated with bottom friction of mainly along-shelf currents. The non-zero shear observed in autumn and in winter regularly lead to marginal stability in the water column here. We note the relatively high noise level in shear-data and a lack of information on the potential influence of salinity stratification and of convective overturning possibly creating unrealistically low gradient Richardson number Ri → 0 (Fig. 3e). On the other hand, from day 320 onwards internal wave motions are not absent, and marginal stability plus internal wave turbulence do occur as will become clear in details below. With the transition to weaker stratification, the amplitude of acoustic echo intensity decreases (Fig. 3f). Large energetic turbulence in a stratified fluid may also affect the acoustic amplitude. Strong echo intensities are largely associated with strong southwestward along-shelf flow and sometimes with offshelf flow, but they are also affected to a lesser extent by periodic onshelf flows and diurnal zooplankton motions (like around day 425).

Although in winter true vertical overturning is found over the entire range of observations, generally due to free convection presumably driven by surface cooling and occasional internal wave breaking, this period is more complicated to analyze than the autumn period. This is because in winter turbulence quantification is not always possible when temperature becomes an unreliable tracer for density variations because of the salinity-compensated intrusions. Therefore, the detailed description periods are mainly from the first third of the record, when stratification dominates and internal wave effects are expected to be strongest.

b. Detailed observations of cross-shelf motions

Since we hypothesized that sediment waves in the Llobregat prodelta are transverse bedforms, we consider in some detail internal wave motions that propagate cross-shelf. Despite the relatively weak cross-shelf currents of amplitudes of 0.1-0.2

m s^{-1}, these flows are always turbulent. This follows from the high estimated bulk Reynolds number Re = UL/ν ≈ O(10^5-10^6), using L = 1-10 m for length-scale and ν = 1.5×10^{-6} m^2s^{-1}, the kinematic viscosity. Distinct periodicities in occurrence of onshelf bores are hard to find, cf. Figure 3c, and spectra (not shown) demonstrate a broad band of elevated kinetic energy between about 0.05 cycles per day (cpd) and the inertial frequency (0.76 cpd).

In the autumn example given in Figure 5 (day 303; 31 October), the stratification is pushed close to the bottom by offshelf turbulent currents, before being lift up by an onshelf propagating turbulent bore with high-frequency internal waves from about 300 s initially to 800 s later propagating along the strongest density interface between 10 and 15 m from the bottom (Fig. 5a). As is common for onshelf propagating bores, e.g. van Haren and Gostiaux (2012), largest turbulence is found just before the bore's front arrival (Fig. 5e) and attributable to convective instabilities associated with highly nonlinear wave deformation (van Haren and Gostiaux, 2016) mainly, with effective interfacial internal wave shear and shear-driven mixing across the interface after the bore's front passage on day 303.46. Largest interfacial internal waves with opposite currents above and below occur between days 303.60 and 303.68. They have a frequency close to the buoyancy frequency of the interior. Shortest internal waves, e.g. between days 303.50 and 303.55 have a frequency close to the local interfacial buoyancy frequency. This shear-driven mixing is due to Kelvin-Helmholtz ('KH') billows (the largest here at days 303.69 and 303.73, indicated by the arrows, 5-6 hours after the front). With typical advection (particle) speeds of 0.12 m s^{-1} and assuming a critical bore so that the phase (propagation) speed equals the particle speed, the high-frequency internal waves have lengths of 25-120 m. This matches the sediment wave lengths observed in the Llobregat prodeltaic deposits at similar water depths and onshelf from the mooring site (Fig. 1). The cooler water advected onshelf has less acoustic reflective material than the warmer waters above (Fig. 5d). An exception is the progressively increase in near-bottom echo intensity, which seems related to the action of small-scale internal waves trailing the front, especially those after day 303.54. Averaged over time-depth intervals of 10 h and 37.5 m, mean turbulence parameter values are $[<\varepsilon>] = 8\pm4\times10^{-7}$ m^{2}s^{-3}, $[<K_z>] = 1.8\pm0.7\times10^{-3}$ m^{2}s^{-1} (determined after averaging the fluxes), $[<N>] = 9.6\pm1\times10^{-3}$ s^{-1} (determined after averaging N^2), while the shortest internal wave period (from the maximum buoyancy frequency) is 125 s. The latter value is a separation value between freely propagating interface internal waves, which must have periods shorter than this value, and turbulent overturns, which can have shorter time-scales. Such mean turbulence values are typical for internal waves breaking over deep-ocean topography (van Haren et al., 2013; 2015) and 100 times larger than the weak turbulent mixing in the ocean interior (e.g., Gregg, 1989).

The example from about a month later (day 332, 29 November) shows a larger onshelf propagating bore with more abundant KH-billow activity (Fig. 6). Overall mean turbulence characteristics are about the same, roughly to within a factor of two as those for Figure 5, as 4 h; 37.5 m mean values are $[<\varepsilon>] = 1.1\pm0.5\times10^{-6}$ m^{2}s^{-3}, $[<K_z>] = 1.0\pm0.4\times10^{-3}$ m^{2}s^{-1}, $[<N>] = 1.5\pm0.2\times10^{-2}$ s^{-1}, with the shortest high-frequency internal wave period developed at the strongest density interface being 94 s. Temperature stratification, and especially also current shear of onshelf moving waters below offshelf moving waters, are thus larger with respect to Figure 5 that the interface between relatively warm and cool waters demonstrates a 10-20 m high zone of continual KH-billows overturning: small-scale internal waves breaking and generating turbulent exchange. The smallest billows are observed near the frontal nose, but these, together with 'secondary' billows at the edge of large billows around day 332.68, cause largest effective mixing. This confirms previous findings of the importance of secondary instabilities, as found in observations in estuaries (Geyer et al., 2010). Although the shear-induced KH-billows mainly overturn the interior stratification, their wavy patterned associated motions do reach the bottom (as far as can be judged from instrumentation down to 5 m above the bottom).

c. Detailed observations of winter convection

In the winter when stratification is strongly reduced, turbulence is dominated by convection that does reach the bottom (Fig. 7). The inertial period ('T_f'; indicated by the horizontal red bar in Fig. 7a) is visible in the clearer stratified waters moving in with onshelf motions. Internal wave motions are reduced, but inertial motions may couple with the weak stratification and also generate convection associated with KH-billows (Fig. 8). Even in the (weakly) stratified waters, convective tubes are observed across the entire range of observations (Fig. 8a,b). These seem to have some periodicity, but the spectrum appears a (sloping) continuum, rather than peaking around particular frequencies (not shown). When shear is relatively weak, as around day 384.9, turbulence is relatively weak although short-term overturns do cause dissipation rate variations over a range of three orders of magnitude. When convection coincides with stronger shear at the transition between offshelf flow being replaced by onshelf flow higher-up, as on day 385.5 ff., large KH-billows associate with convection penetrating towards the bottom (Fig. 8c). Using the autumnal temperature-density relationship as a conservative estimate of the coarsely resolved winter CTD-data (Fig. 2), the 1.5 d; 37.5 m (Fig. 7) mean turbulence parameter values are $[<\varepsilon>] = 5\pm2\times10^{-7}$ m^{2}s^{-3}, $[<K_z>] = 5\pm2\times10^{-3}$ m^{2}s^{-1}, $[<N>] = 4.3\pm0.5\times10^{-3}$ s^{-1}, with the shortest internal wave period being 163 s. The turbulence values are thus half an order of magnitude larger than those for Figures 5 and 6.

4. Discussion

4.1. Critical slope and internal waves (general considerations).

Previous optics observations on continental margins suggested a correlation between the bottom-source of ‘nepheloid layers’, attributed to enhanced suspended sediment dispersed along isopycnals into the interior, and ‘critical internal wave reflection’ zones (e.g., Cacchione and Drake, 1986; McPhee-Shaw, 2006). In such a zone a match is expected between the bottom-slope angle and the angle of the dominant internal wave propagation. Theoretically, a freely propagating internal gravity wave impinging upon a bottom slope equaling its propagation angle will cause energy condensation near the bottom that may result in wave breaking. The internal wave angle α depends on the wave frequency σ, the inertial frequency $f = 2\Omega\sin\varphi$, $\mathbf{\Omega}$ the Earth rotational vector and φ the latitude, and the buoyancy frequency N: $\sin^2\alpha = (\sigma^2 - f^2)/(N^2 - f^2)$, (LeBlond and Mysak, 1978). Under normal stratification conditions outside near-homogeneous (‘well-mixed’) waters, freely propagating internal waves exist in the band $f \leq \sigma \leq N$.

In the ocean however, first, N varies in space and in time, so that a particular wave angle, the internal wave beam and the loci of ‘critical reflection’ vary accordingly. Second, three-dimensional ‘3D’-internal wave propagation also requires a 3D knowledge of the slopes of the bottom-topography on all relevant scales, which is only obtainable via high-resolution multi-beam mapping. Third, turbulent bores have been observed to occur once every four days related with storm-induced sub-inertial motions in the Faeroe-Shetland Channel (Hosegood et al., 2004) and once a day related with trapped diurnal tides in the Rockall Channel (van Haren et al., 2014). Both periodicities are ‘sub-inertial’ $\sigma < f$ and cannot support freely propagating internal waves.

More in general, strongest internal wave breaking and most vigorous bores seem to occur above super-critical, that is steep, slopes where the bottom slope exceeds the dominant (inertial, tidal) internal wave slope (van Haren et al., 2015; confirmed via DNS-modelling, Sarkar, pers. comm.). Thus, the slope steepness seems to matter more for internal wave breaking than its critical matching of particular internal wave source (near-inertial) frequency. Above such steep slopes, internal waves at higher frequencies well inside the internal wave band may become critical. Near-bottom onshelf propagating turbulent bores are observed to affect fine sediment transport (Hosegood et al., 2004; Bourgault et al., 2014). The associated trailing high-frequency internal waves that were also observed, are here considered to be important for bedforms development.

Internal waves and larger scale currents exhibit vertical current shear, which destabilizes the stratification. The relation between shear and stratification is subtle: the larger the stable stratification the more destabilizing shear it can support, up to the point of marginal stability, see Polzin (1996) and Pinkel and Anderson (1997) for ocean data. In shallow seas, then main drivers of marginal stability are inertial motions due to the rotation of the earth in combination with small-scale internal waves (van Haren et al., 1999). The question is, how such large- and small-scale internal waves, and, possibly, their breaking, affect the development of the sediment waves observed here.

A major conjecture for internal wave development in continental shelf environments is the vertical density stratification in the water column, which exists for most of the time except for brief periods in winter and although with varying strength at varying depths. The stable density stratification affects the characteristics of turbulence by hampering the larger overturning scales in the vertical so that the essentially 3D-nature of the turbulence becomes 2- or 2.5D. This results in different 'stratified' Ekman dynamics, in which frictional effects are balanced by the rotation of the earth (Ekman, 1905), the layers of varying density mutually behaving much more slippery than homogeneous layers so that bottom frictional turbulence is not well communicated to the upper layer, the layer to which the along-shelf flow is then mostly confined here.

4.2. Matching internal waves with sediment waves in the Llobregat prodelta.

The Llobregat prodelta sediment waves are a phenomenon at only 1-3 km from the coast. They exist in an area where the overlying water flows, the currents, are observed to attain amplitudes exceeding 0.6 m s^{-1}. However, as the currents are mainly directed parallel to the coast, parallel to the bottom slope and parallel to the sediment wave crests, other mechanisms for the interaction between water motion and sediment wave formation are to be sought.

In other Mediterranean prodeltas sediment waves were interpreted caused by high density hyperpycnal flows (e.g., Lobo et al. 2014). However, the location of the sediment waves with respect to the river mouth, and their morphology and internal structure suggest a different origin for the Llobregat sediment waves (Urgeles et al., 2011). These authors compared sediment waves developed in several prodeltaic areas of the Mediterranean Sea and concluded that the most likely mechanisms for the genesis of the Llobregat sediment waves are internal waves. Similar fine-grained, sandy and carbonate sediment wave fields developed in continental slopes worldwide have been attributed to internal waves (e.g., Karl et al, 1986; Ediger et al., 2002; Reeder et al., 2011; Bøe et al., 2015; Belde et al., 2015).

The sediment waves and seafloor structure of the Llobregat prodelta has also similarities with that of the Gulf of Valencia continental slope (Ribó et al. 2016a,b), although in this case the bedforms are much smaller (about 1 versus 10 m height, respectively). These muddy sediment waves are located between 35 and 90 m depth in the Llobregat and between 250 and 850 m depth in the Gulf of Valencia. However, both are found just at the seaward side of the steepest part of the local (continental) slope, at the foreset region of both types of prograding clinoforms (i.e., a prodeltaic mud wedge vs. a continental margin). In the Gulf of Valencia, internal waves have been observed at a dominant local inertial period which is modulated by an about 11 day periodic, baroclinic unstable boundary current. When this current is strong and eastward, the upslope phase of inertial wave generates convective turbulence which reaches closest to the bottom and therefore can affect sediment dispersal. In late winter, equally strong shear-induced turbulence in 50 m high KH-billows is forced by off-slope moving cooler bottom water, which is suddenly flushed over the promontory into the basin (van Haren et al., 2013). The region in the Gulf of Valencia slope with the highest sediment waves (~50 m in height) coincided with the water depths where the KH-billows were observed, both displaying equivalent amplitudes, an aspect considered by Ribó et al. (2016a) to attribute their formation to internal waves.

The density stratification also supports internal waves having wavelengths between about 1 km at near-inertial frequencies and about 10 m at near-buoyancy frequencies. Here, high-frequency internal waves are observed to have lengths of 50-100 m that match those of the local sediment waves. (Anti-)dune formation is expected when overlying water waves match the sediment waves in wavelength. At this stage one cannot rule out the effects of surface waves because they only can weakly reach the 35-90 m deep bottom during the strongest storms. In fact, the absence of undulations <35 m water depth and the evidence of erosion in the shallowest sediment waves have been interpreted by Urgeles et al. (2011) as an effect of storms reshaping of the sediment wave field.

The present observational experiment has been performed in the autumn-spring half year to study near-bottom internal waves and turbulence (and flows). It is thought that the spring-summer period provides very strong (temperature dominated) stratification. Internal waves supported by such large stratification are expected to affect the bottom less when they are in the upper half of the water column, except perhaps in shallower waters closer to the shore than the mooring location.

The autumn/winter period is observed to be characterized by mixing by the strongest storms in the area and by onshelf propagating internal bores when stratification is still non-negligible but pushed down to within 5-10 m from the bottom. The bores are turbulent, but mainly shear-driven and the associated KH-billows trailing the front are accompanied by high-frequency internal waves with wavelengths that match those of the sediment waves. The bores are the highly nonlinear relaxation following an instability that is either created by near-inertial internal waves or Ekman layer dynamics (over a sloping bottom with stratified waters above) of sub-inertial 3-7 d periodic southwest currents, as in the Faroer-Shetland Channel (Hosegood and van Haren, 2003).

The variable but relatively short periodicity of 3-7 days is typical for atmospheric effects near the coast in the northwestern Mediterranean (e.g., Font, 1990; Jimenez et al, 1999; Rubio et al, 2009; Ribó et al., 2015), while it is shorter than generally considered typical (10-20 days; e.g., Crépon et al., 1982; Albérola et al., 1995), for the

Northern Current which flows along the continental slope but further seaward. The bores are termed 'gravity currents' by Venayagamoorthy and Fringer (2012) because of their intruding nature. However, they contrast with the more general turbidity 'gravity' currents, which have been modelled to generate sediment waves (Hoffmann et al., 2015), but which essentially flow offshelf. These are not observed here.

The winter/spring period is characterized by strong convective turbulence mixing waters to near-homogeneity and either (just) preceding the above onshelf propagating bores during the offshelf flow phase or driven by atmospheric surface cooling. Convective turbulence is found to be a quasi-regular process, but considerably less regularly varying than high-frequency internal waves. Additionally, the scales of convection cells are not found to match the scales of sediment waves.

5. Conclusions

Analyses of time series collected by a near-bottom array of high-resolution temperature sensors moored at 81 m water depth, seaward of an extensive sediment wave field in the Llobregat River prodelta, provided a comprehensive view of the internal wave and turbulence activity in this region during the autumn-spring transition and insights of its potential role for the development of sediment wavesn. The results presented in this study support the following conclusions:

- Strong stratification can become depressed to very close to the bottom in autumn and supports high-frequency internal waves some of which break under shear. The associated turbulence matches that of deep-ocean large internal waves breaking at sloping topography and is 100 times larger than internal wave induced turbulence in the ocean interior.

- During weak stratification in winter, large convective turbulence is observed which is estimated to be half an order of magnitude larger than the shear-induced turbulence in autumn. Conservative estimate: it can be larger
- The high-frequency internal waves close to the buoyancy frequency trail observed onshelf propagating frontal bores with relatively weak (0.1-0.2 m s^{-1}) current amplitudes. The fronts pass irregularly, roughly with inertial periodicity or a periodicity of 3-7 days, depending on the main driver. The associated trailing interfacial waves have wavelengths matching those of the sediment waves. Their shear-induced mixing is observed as a series of Kelvin-Helmholtz billows that under critical bore conditions. These instabilities and the high-frequency waves most likely interact with the sediment waves, presumably causing local resuspension and or inhibiting particle deposition in the steep flank of the up-slope migrating sediment wave, contributing to their generation and maintenance through time.

Acknowledgments. This research was supported by the project FORMED (CGL2012-33989), funded by the Spanish Ministry of Economy and Competitiveness. We thank J. Guillen for initiating this project. We thank the captain and the crew of the R/V Garcia del Cid for their kind assistance during oceanographic cruises. We thank M. Laan for all his enthusiastic development of NIOZ-temperature sensors and D. A. Cacchione for inspiring comments regarding the potential role of high-frequency internal waves. R. Urgeles kindly provide the multibeam bathymetry of the Llobregat prodelta used in Figure 1.

References

Abarbanel, H.D.I., Holm, D.D., Marsden, J.E., Ratiu, T., 1984. Richardson number criterion for the nonlinear stability of three-dimensional stratified flow. Physical Review Letters 52, 2352-2355.

Albérola, C., Millot, C., Font, J., 1995. On the seasonal and mesoscale variabilities of the northern current during the PRIMO-0 experiment in the western Mediterranean. Oceanologica Acta 18, 163-192.

Alexander J., Bridge, J.S., Cheel, R.J., LeClair, S.F., 2001. Bedforms and associated sedimentary structures formed under supercritical water flows over aggrading sand beds. Sedimentology 48, 133-152.

Belde, J., Back, S., Reuning, L., 2015. Three-dimensional seismic analysis of sediment waves and related geomorphological features on a carbonate shelf exposed to large amplitude internal waves, Browse Basin region, Australia. Sedimentology 62, 87-109.

Berndt, C., Cattaneo, A., Szuman, M., Trincardi, F., Masson, D., 2006. Sedimentary structures offshore Ortona, Adriatic Sea—Deformation or sediment waves? Marine Geology 234, 261-270.

Bøe R., et al., 2015. Sand waves and sand transport on the Barents Sea continental slope offshore northern Norway. Marine and Petroleum Geology 60, 34-53.

Bourgault, B., Morsilli, M., Richards, C., Neumeier, U., Kelley, D.E., 2014. Sediment resuspension and nepheloid layers induced by long internal solitary waves shoaling orthogonally on uniform slopes. Continental Shelf Research 72, 21-33.

Cacchione, D.A., Drake, D.E., 1986. Nepheloid layers and internal waves over continental shelves and slopes. Geo-Marine Letters 16, 147-152.

Checa, A., Díaz, J.I., Farrán, M., Maldonado, A., 1988. Sistemas deltaicos holocenos de los ríos Llobregat, Besós y Foix: modelos evolutivos transgresivos. Acta Geològica Hispànica 23, 241-255.

Correggiari, A., Trincardi, F., Langone, L., Roveri, M., 2001. Styles of failure in Late Holocene highstand prodelta wedges on the Adriatic shelf. Journal of Sedimentary Research 71, 218-236.

Crépon, M., Wald, L., Monget, J.M., 1982. Low-frequency waves in the Ligurian Sea during December 1977. Journal of Geophysical Research 87, 595-600.

Ediger, V., Velegrakis, A. F., Evans, G., 2002. Upper slope sediment waves in the Cilician Basin northeastern Mediterranean. Marine Geology 192, 321-333.

Ekman, V.W., 1905. On the influence of the Earth's rotation on ocean-currents. Arkiv för matematik, astronomi och fysik 2(11), 1-52.

Faugères, J.C., et al., 2002. Multi-process generated sediment waves on the Landes Plateau (Bay of Biscay, North Atlantic). Marine Geology 182, 279-302.

Fernández-Salas, L.M., Lobo, F.J., Sanz, J.L., Díaz-del-Río, V., García, M.C., Moreno, I., 2007. Morphometric analysis and genetic implications of pro-deltaic sea-floor undulations in the northern Alboran Sea margin, western Mediterranean Basin. Marine Geology 243, 31–56.

Flagg, C.N., Smith, S.L., 1989. On the use of the acoustic Doppler current profiler to measure zooplankton abundance. Deep-Sea Research A 36, 455-474.

Flood, R.D., 1988. A lee wave model for deep-sea mudwave activity. Deep-Sea Research I 35, 973-983.

Font, J., Salat, J., Julià, A., 1990. Marine circulation along the Ebro continental margin. Marine Geology 95, 165–177.

Gargett, A., Gardner, T., 2008. Determining Thorpe scales from ship-lowered CTD density profiles. Journal of Atmospheric and Oceanic Technology 25, 1657-1670.

Geyer, W.R., Lavery, A.C., Scully, M.E., Trowbridge, J.H., 2010. Mixing by shear instability at high Reynolds number. Geophysical Research Letters 37, L22607, doi:10.1029/2010GL045272.

Gregg, M.C., 1989, Scaling turbulent dissipation in the thermocline. Journal of Geophysical Research 94, 9686-9698.

Grifoll, M., Aretxabaleta, A.L., Pelegrí, J.L., Espino, M., Warner, J.C., Sánchez-Arcilla, A., 2013. Seasonal circulation over the Catalan inner-shelf (northwest Mediterranean Sea). Journal of Geophysical Research 118, 5844-5857, doi:10.1002/jgrc20403.

Hoffmann, G., Nasr-Azadani, M.M., Meiburg, E., 2015. Sediment wave formation caused by erosional and depositional turbidity currents: a numerical investigation. Proceedings IUTAM 15, 26-33.

Hosegood, P., van Haren, H., 2003. Ekman-induced turbulence over the continental slope in the Faeroe-Shetland Channel as inferred from spikes in current meter observations. Deep-Sea Research I 50, 657-680.

Hosegood, P., Bonnin, J., van Haren, H., 2004. Solibore-induced sediment resuspension in the Faeroe-Shetland Channel. Geophysical Research Letters 31, L09301, doi:10.1029/2004GL019544.

IOC, SCOR, IAPSO, 2010. The international thermodynamic equation of seawater – 2010: Calculation and use of thermodynamic properties. Intergovernmental Oceanographic Commission, Manuals and Guides No. 56, UNESCO, Paris, France, 196 pp.

Jiménez, J.A., et al., 1999. Water and sediment fluxes on the Ebro delta shoreface. On the role of low frequency currents. Marine Geology 157, 219-239.

Karl, H.A., Cacchione, D.A., Carlson, P.R., 1986. Internal-wave currents as a mechanism to account for large sand waves in Navarinsky canyon head, Bering Sea. Journal of Sedimentary Petrology 56, 706-714.

Klymak, J.M., Moum., J.N., 2003. Internal solitary waves of elevation advancing on a shoaling shelf. Geophysical Research Letters 30, 2045, doi:10.1029/2003GL017706.

LeBlond, P.H., Mysak, L.A., 1978. Waves in the Ocean. Elsevier, New York, 602 pp.

Lee, H.J., Syvitski, J.P.M., Parker, G., Orange, D., Locat, J., Hutton, E.W.H., Imran, J., 2002. Distinguishing sediment waves from slope failure deposits: field examples, including the “Humboldt slide”, and modelling results. Marine Geology 192, 79-104.

Lobo, F.J., et al., 2014. Spatial variability of prodeltaic undulations on the Guadalfeo River prodelta: support to the genetic interpretation as hyperpycnal flow deposits. Marine Geophysical Research 36, 309-333.

McPhee-Shaw, E.E., 2006. Boundary- Interior Interactions: Reviewing the idea that internal-wave mixing enhances lateral dispersion near continental margins. Deep-Sea Research II 53, 42-59.

Millot, C., Crépon, M., 1981. Inertial fluctuations on the continental shelf of the Gulf of Lions-Observations and theory. Journal of Physical Oceanography 11, 639–657.

Millot, C., 1999. Circulation in the western Mediterranean Sea. Journal of Marine Systems 20, 423-442.

Pinkel, R., Anderson, S., 1997. Shear, strain, and Richardson number variations in the thermocline. Part I: statistical description. Journal of Physical Oceanography 27, 264-281.

Plueddemann, A.J., Pinkel, R., 1989. Characterization of the patterns of diel migration using a Doppler sonar. Deep-Sea Research A 36, 509-530.

Polzin, K., 1996. Statistics of the Richardson number: mixing models and finestructure. Journal of Physical Oceanography 26, 1409-1425.

Puig, P., Palanques, A., Guillén, J., 2001. Near-bottom suspended sediment variability caused by storms and near-inertial internal waves on the Ebro mid continental shelf (NW Mediterranean). Marine Geology 178, 81-93.

Puig, P., Ogston, A.S., Guillén, J., Fain, A.M.V., Palanques, A., 2007. Sediment transport processes from the topset to the foreset of a crenulated clinoform (Adriatic Sea). Continental Shelf Research 27, 452-474.

Reeder, D.B., Ma, B.B., Yang, Y.J. 2011. Very large subaqueous sand dunes on the upper continental slope in the South China Sea generated by episodic, shoaling deep-water internal solitary waves. Marine Geology 279, 12-18.

Ribó, M., Puig, P., van Haren, H., 2015. Hydrodynamics over the Gulf of Valencia continental slope and their role in sediment transport. Deep Sea Research I 95, 54-66.

Ribó, M., et al., 2016a. Morphobathymetric analysis of the large fine-grained sediment waves over the Gulf of Valencia continental slope (NW Mediterranean). Geomorphology 253, 22-37.

Ribó, M., Puig, P., Urgeles, R., Van Rooij, D., Muñoz, A., 2016b. Spatio-temporal evolution of the sediment waves developed on the Gulf of Valencia margin (NW Mediterranean) during the Plio-Quaternary. Marine Geology 378, 276-291.

Rubio, A., Taillandier, V., Garreau, P., 2009. Reconstruction of the Mediterranean northern current variability and associated cross-shelf transport in the Gulf of Lions from satellite-tracked drifters and model outputs. Journal of Marine Systems 78, S63-S78.

Salat, J., Tintore, J., Font, J., Wang, D.-P., Vieira, M., 1992. Near-inertial motion on the shelf-slope front off northeast Spain. Journal of Geophysical Research 97, 7277-7281.

Thorpe, S.A., 1977. Turbulence and mixing in a Scottish loch. Philosophical Transactions of the Royal Society London A 286, 125-181.

Trincardi, F., Normark, W.R., 1988. Sediment waves on the Tiber pro-delta slope. Geo-Marine Letters 8, 149-157.

Turner, J.S., 1979. Buoyancy effects in fluids. Cambridge University Press, Cambridge U.K., 368 pp.

Urgeles, R., et al., 2007. Sediment undulations on the Llobregat prodelta: signs of early slope instability or bottom current activity? Journal of Geophysical Research 112, B05102.

Urgeles, R., et al., 2011. A review of undulated sediment features on Mediterranean prodeltas: distinguishing sediment transport structures from sediment deformation. Marine Geophysical Research 32, 49-69.

van Haren, H, 2014. Internal wave – zooplankton interactions in the Alboran Sea (W-Mediterranean). Journal of Plankton Research 36, 1124-1134.

van Haren, H., 2017. Internal waves and bedforms. In: Atlas of bedforms in the western Mediterranean. In: Guillén, J., Acosta, J., Chiocci, F.L., Palanques, A., eds., Springer, pp. 25-28.

van Haren, H., Gostiaux, L., 2012. Detailed internal wave mixing observed above a deep-ocean slope. Journal of Marine Research 70, 173-197.van Haren, H., Gostiaux, L., 2016. Convective mixing by internal waves in the Puerto Rico Trench. Journal of Marine Research 74, 161-173.

van Haren, H., Maas, L., Zimmerman, J.T.F., Ridderinkhof, H., Malschaert, H., 1999. Strong inertial currents and marginal internal wave stability in the central North Sea. Geophysical Research Letters 26, 2993-2996.

van Haren, H., Laan, M., Buijsman, D.-J., Gostiaux, L., Smit, M.G., Keijzer, E., 2009. NIOZ3: independent temperature sensors sampling yearlong data at a rate of 1 Hz. IEEE Journal of Oceanic Engineering 34, 315-322.

van Haren, H., Ribó, M., Puig, P., 2013. (Sub-)inertial wave boundary turbulence in the Gulf of Valencia. Journal of Geophysical Research 118, 2067-2073, doi:10.1002/jgrc.20168.

van Haren, H., Mienis, F., Duineveld, G.C.A., Lavaleye, M.S.S., 2014. High-resolution temperature observations of a trapped nonlinear diurnal tide influencing cold-water corals on the Logachev mounds. Progress in Oceanography 125, 16-25.

van Haren, H., Cimatoribus, A., Gostiaux, L., 2015. Where large deep-ocean waves break. Geophysical Research Letters 42, 2351-2357, doi:10.1002/2015GL063329.

Venayagamoorthy, S.K., Fringer, O.B., 2012. Examining breaking internal waves on a shelf slope sing numerical simulations. Oceanography 25(2), 132-139, http://dx.doi.org/10.5670/oceanog.2012.48.

Verdicchio, G., Trincardi, F., 2006. Short-distance variability in slope bed-forms along the Southwestern Adriatic Margin (Central Mediterranean). Marine Geology 234, 271-292.

Vlasenko, V., Hutter, K., 2002. Numerical experiments on the breaking of solitary internal waves over a slope-shelf topography. Journal of Physical Oceanography 32, 1779-1793.

Wynn, R.B., Stow, D., 2002. Classification and characterisation of deep-water sediment waves. Marine Geology 192, 7-22.

Figure 1. Shaded relief bathymetric map of the Llobregat prodelta outside Barcelona harbour (NW-Mediterranean Sea), showing the positions of the mooring (black pin) and CTD site (white triangle) near the harbour's Sierra buoy (80 m depth). The undular bedforms with crests parallel to the coast are clearly visible shoreward between the buoy and about 35 m depth. The bathymetric survey was conducted in 2004 (R. Urgeles, personal communication).

Figure 2. Lower half of CTD observations around the times of mooring deployment in autumn (blue, green), in winter (purple) and around mooring recovery in spring (black). (a) Conservative Temperature with the range of moored temperature sensors (red bar). (b) Absolute Salinity; the x-axis range matches that of a. in terms of density variation. (c) Conservative Temperature – potential density anomaly referenced to the surface, with linear relationships given by straight (magenta and yellow) lines, resulting in a mean $\delta\sigma_\theta = \alpha\delta\Theta$, $\alpha = -0.26\pm0.02$ kg m^{-3} $°C^{-1}$ the apparent local expansion coefficient. (d) Comparison of the slope of relationships in c. with density from profile data.

Figure 3. Data overview of 170 day time-depth series. Currents are measured using ADCP, temperature using moored high-resolution T-sensors. The vertical purple lines indicate short periods of which details are shown in Figures (F) 5-8. (a) Conservative Temperature. (b) Along-shelf current component (positive towards northeast), hourly smoothed to reduce noise. (c) Cross-shelf current component (positive offshelf), hourly smoothed. Note the different colour-scale compared with b. (d) Vertical current component (positive up), hourly smoothed. Note the different colour-scale compared with b. (e) Gradient Richardson number Ri =

$N^2/|S|^2$. (f) Acoustic echo intensity relative to the time mean at each depth-bin. (g) Vertically averaged (between 5.5 and 42.5 m above the bottom) turbulence dissipation rate inferred from temperature data. Some high values occurring after day 340, e.g. around days 360, 400 and 405, are unrealistic and partially caused by salinity-compensated intrusions (see text).

Figure 4. (a) Local wind speed data (blue) and the gradient of near-bottom temperature data (arbitrary scale) of which peaks demonstrate the occurrence of fronts. (b) Spectra of mid-range kinetic energy, local wind and near-bottom temperature variance.

Figure 5. Autumn 10-h detail-example of transition from offshelf near-bottom flow to onshelf (-u) propagating near-bottom front. (a) Conservative Temperature. Note the smaller range of 1°C, compared with Figure 3a. (b) Cross-shelf current, original (300 s) data. (c) Logarithm of buoyancy frequency from reordered Θ-profiles. (d) Relative acoustic echo intensity. (e) Vertically averaged turbulence dissipation rate.

Figure 6. As Figure 5, but for 4-h observations of onshelf propagating bore four weeks later and including numerous interior (40-60 m) Kelvin-Helmholtz billow overturning across the largest stratification. Note the different 1.9°C range in panel a., compared with Figures 3a,5a.

Figure 7. As Figure 5, but for 1.5-d observations in mid-January of inertial and diurnal convective overturning and offshelf near-bottom currents. Note the different 0.5°C range in panel a., compared with Figures 3a, 5a, 6a. The vertical

purple lines indicate half-hour periods of Figures 8a-c. The horizontal red line indicates one inertial period.

Figure 8. Half-hour zooms of Figure 7a, showing convection reaching the lowest sensors. Note the different colour ranges.

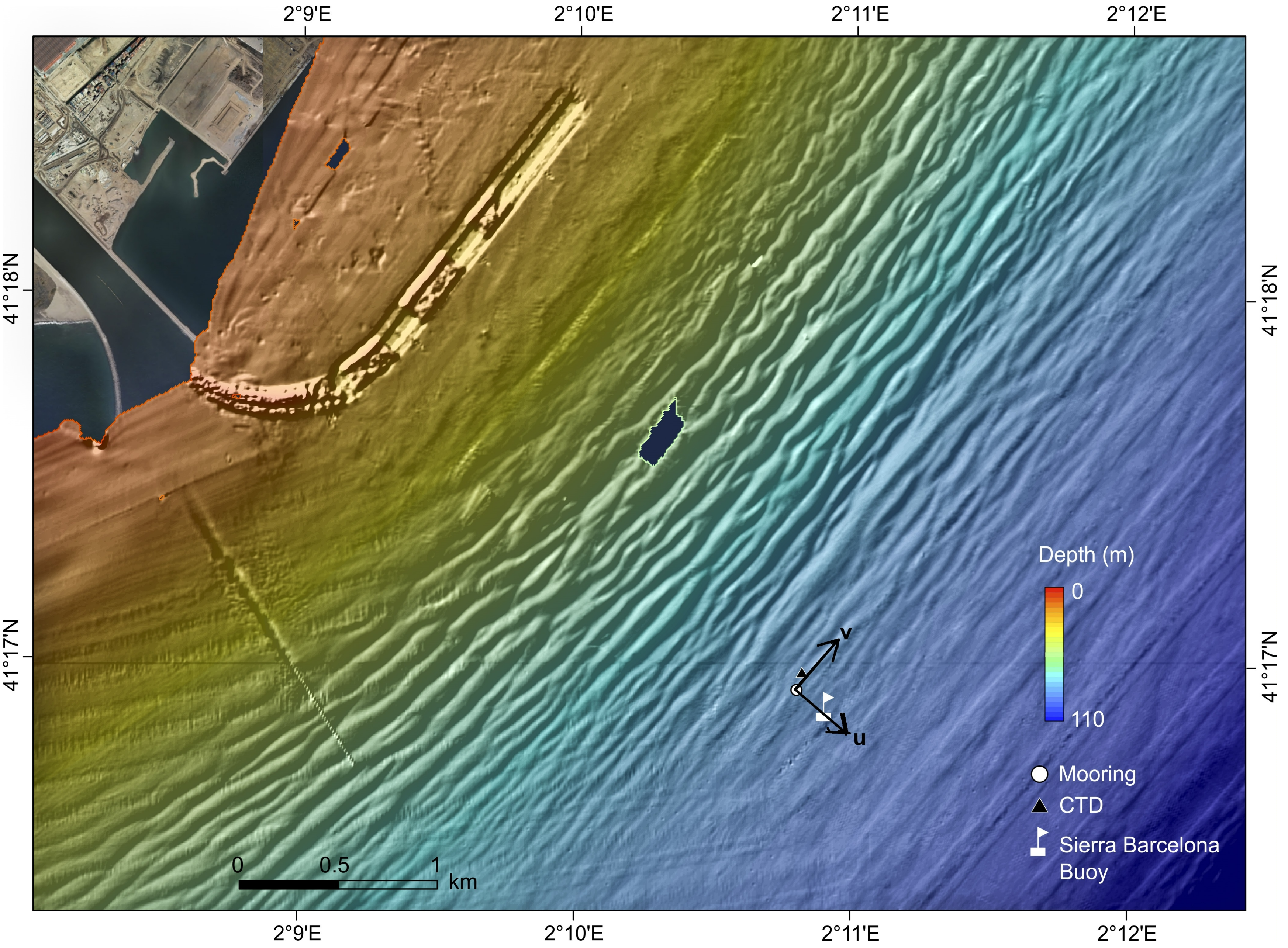
2°9'E
2°10'E
2°11'E
2°12'E
41°18'N
41°17'N
Depth (m)
0
110
v
u
Mooring
CTD
Sierra Barcelona Buoy
0
0.5
1
km

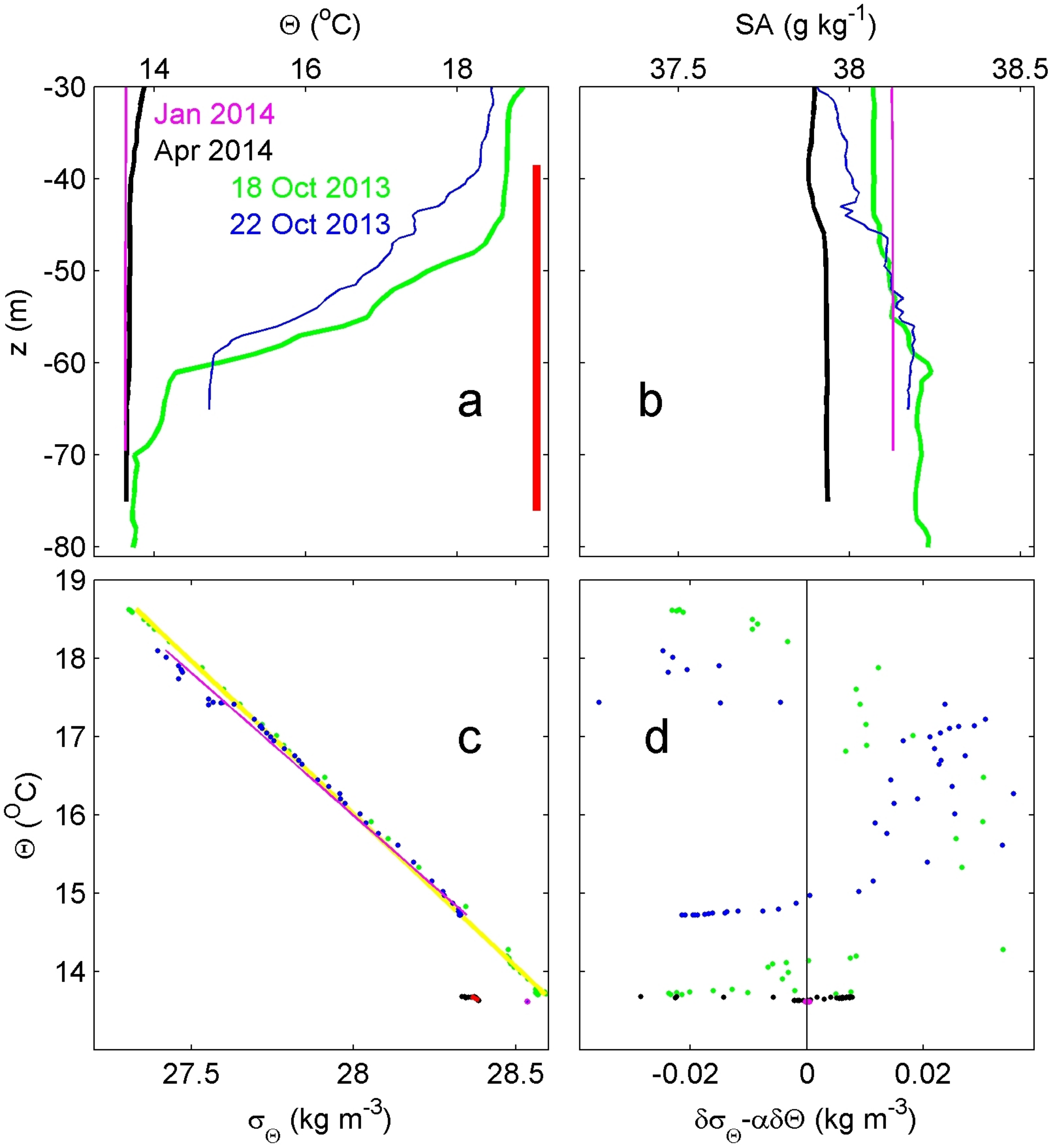
Θ (°C)
14
16
18
SA (g kg^{-1})
37.5
38
38.5
-30
-40
-50
-60
-70
-80
z (m)
Jan 2014
Apr 2014
18 Oct 2013
22 Oct 2013
a
b
19
18
17
16
15
14
Θ (°C)
c
d
27.5
28
28.5
σ$_Θ$ (kg m^{-3})
-0.02
0
0.02
δσ$_Θ$-αδΘ (kg m^{-3})

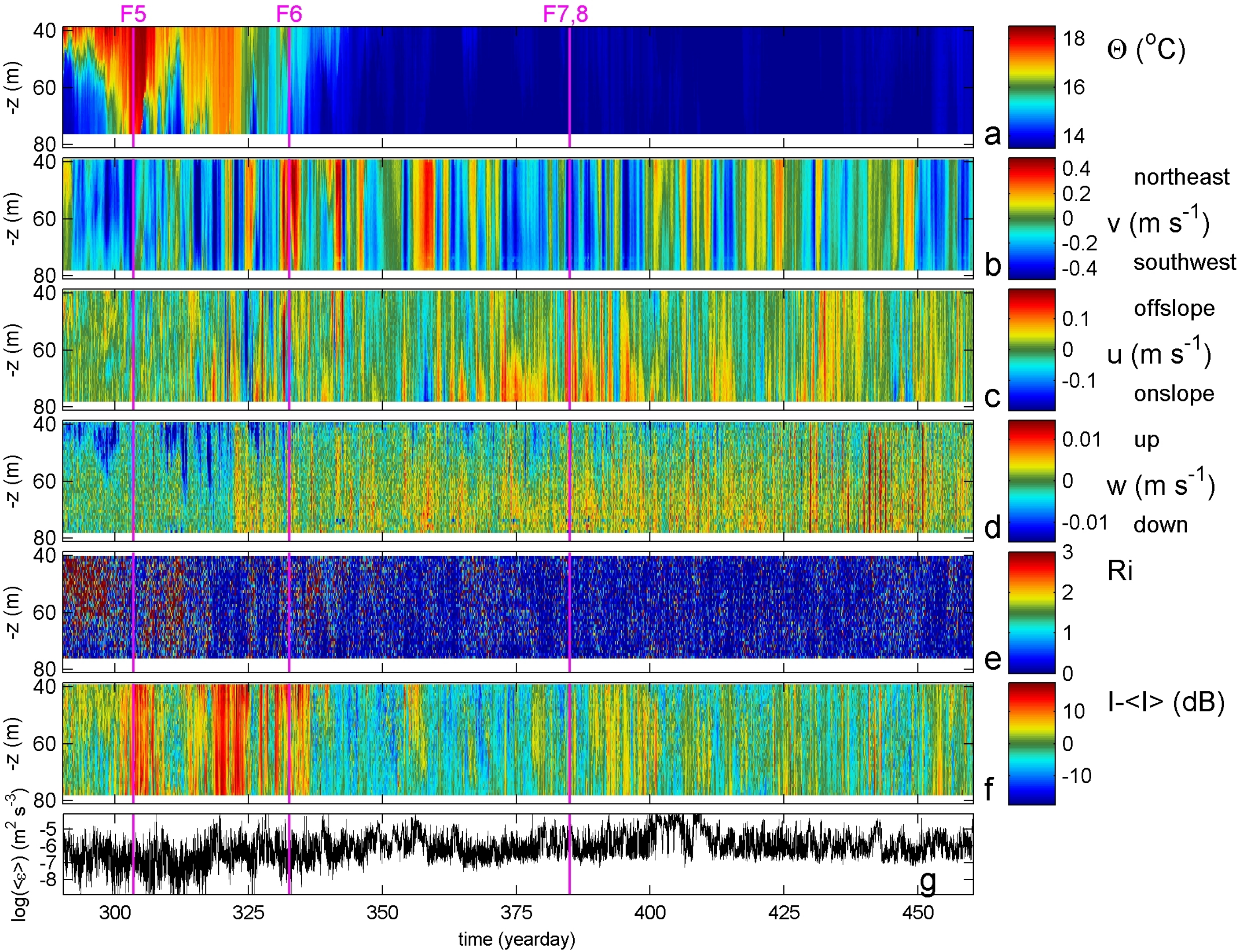
F5
F6
F7,8
-z (m)
40
60
80
a
18
16
14
Θ (°C)
b
0.4
0.2
0
-0.2
-0.4
northeast
v (m s^{-1})
southwest
c
0.1
0
-0.1
offslope
u (m s^{-1})
onslope
d
0.01
0
-0.01
up
w (m s^{-1})
down
e
3
2
1
0
Ri
f
10
0
-10
I-<I> (dB)
g
log(<ε>) (m^2 s^{-3})
-5
-6
-7
-8
300
325
350
375
400
425
450
time (yearday)

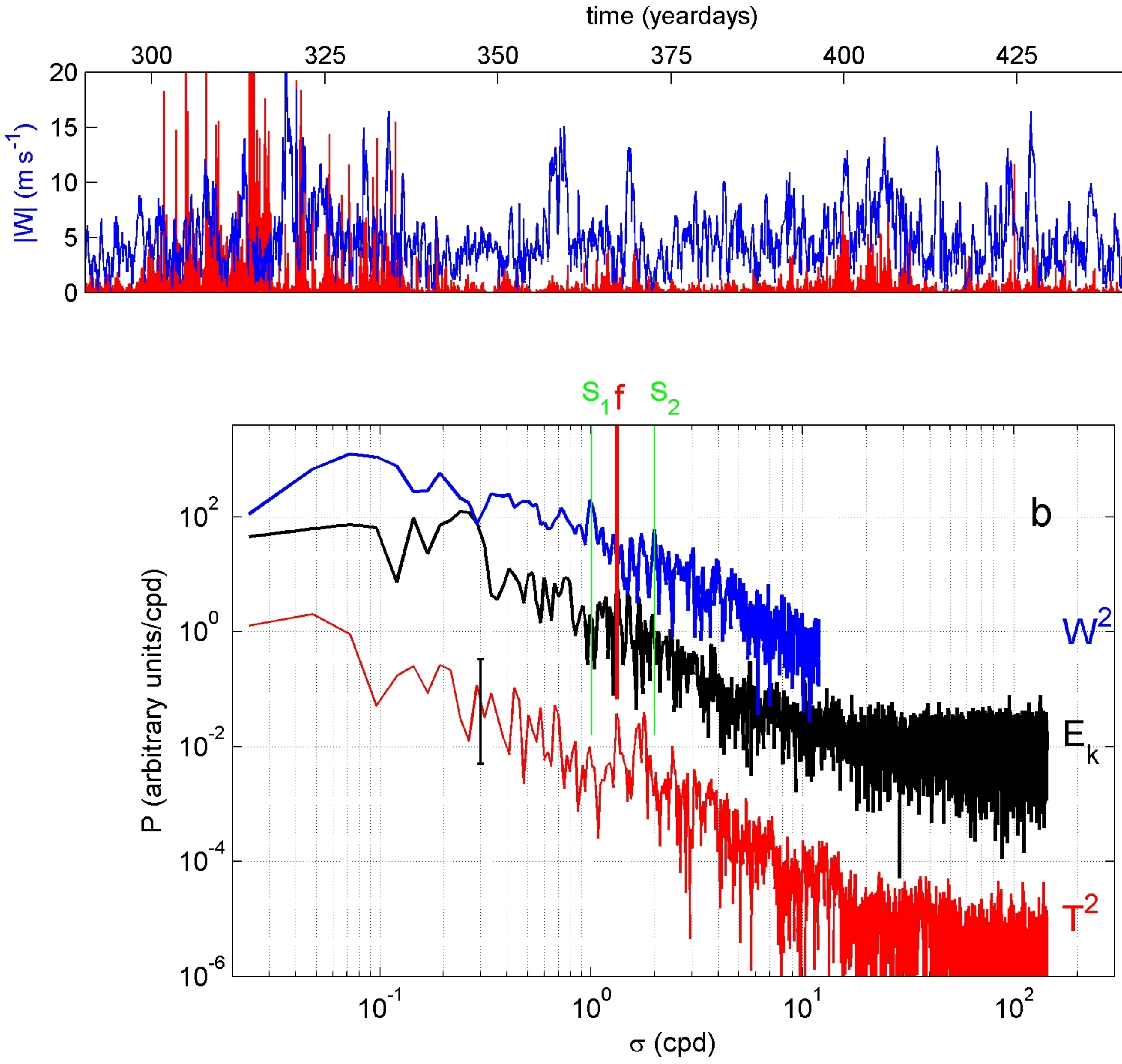
time (yeardays)
300
325
350
375
400
425
450
20
15
10
5
0
|W| (m s^{-1})
a
S$_1$
f
S$_2$
b
10^2
10^0
10^{-2}
10^{-4}
10^{-6}
P (arbitrary units/cpd)
W^2
E$_k$
T^2
10^{-1}
10^0
10^1
10^2
σ (cpd)

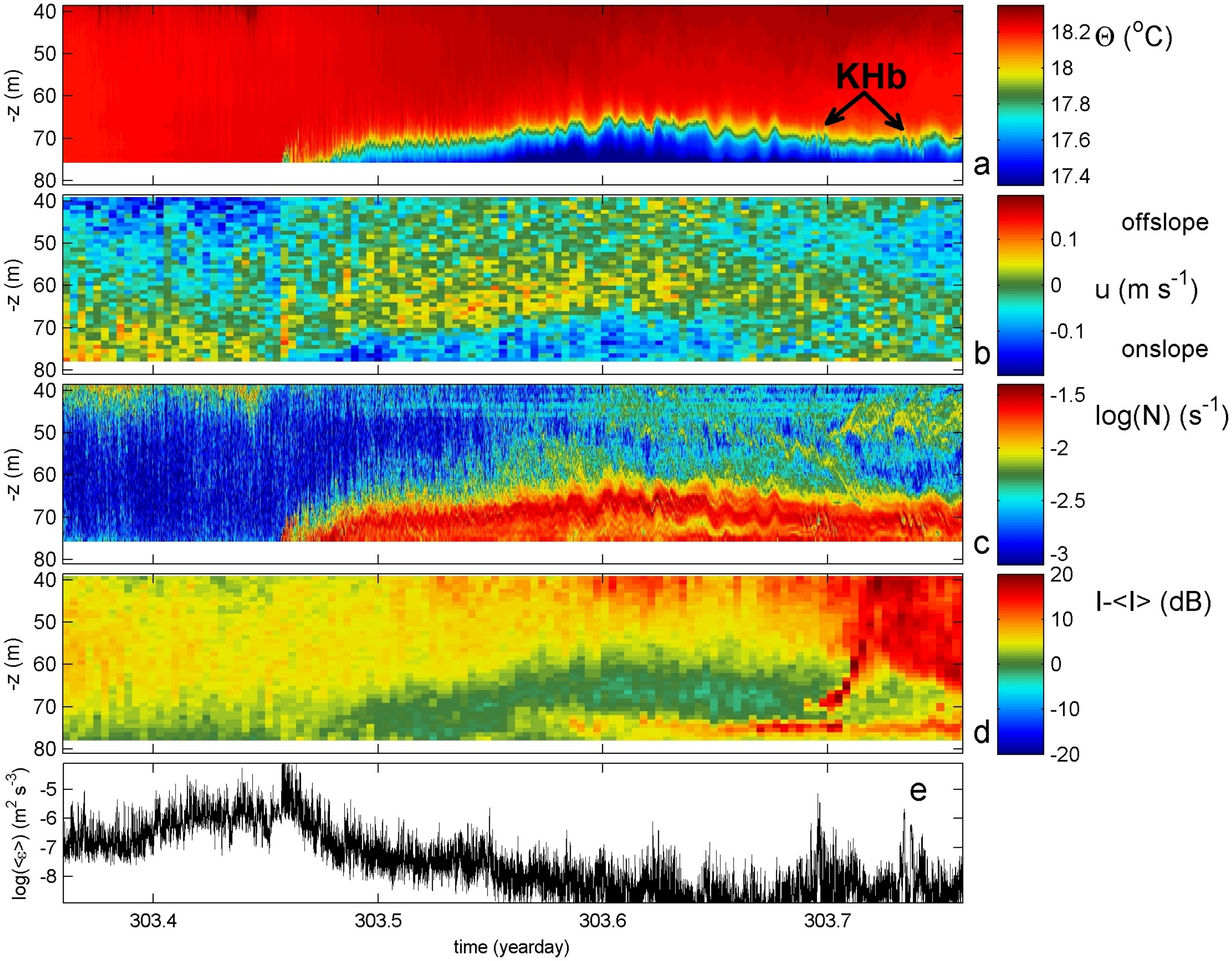

KHb
a
b
c
d
e
-z (m)
40
50
60
70
80
Θ (°C)
18.2
18
17.8
17.6
17.4
offslope
onslope
u (m s^{-1})
0.1
0
-0.1
log(N) (s^{-1})
-1.5
-2
-2.5
-3
I-<I> (dB)
20
10
0
-10
-20
log(<ε>) (m^2 s^{-3})
-5
-6
-7
-8
303.4
303.5
303.6
303.7
time (yearday)

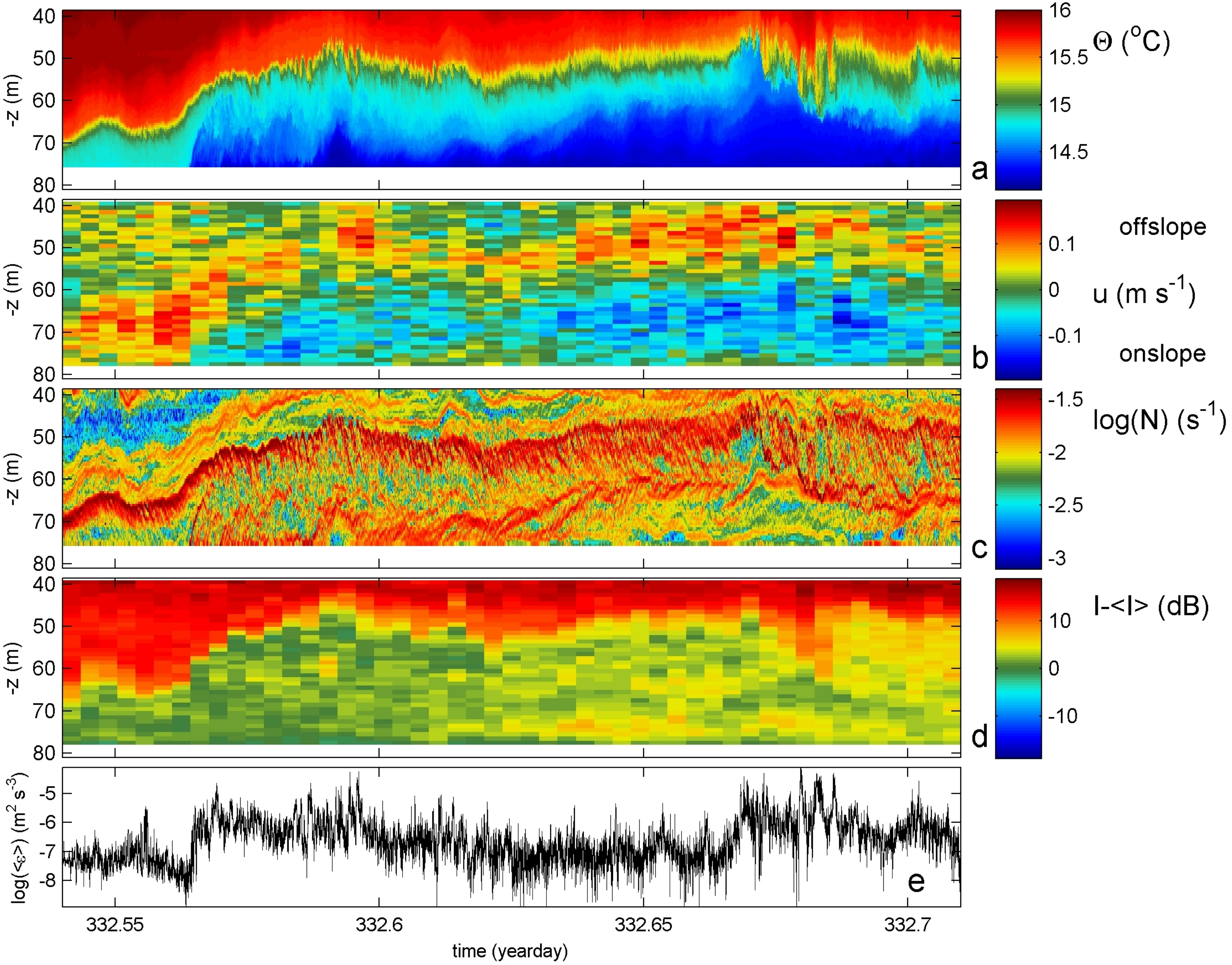

-z (m)
40
50
60
70
80
a
16
15.5
15
14.5
Θ (°C)
b
offslope
0.1
0
-0.1
onslope
u (m s-1)
c
-1.5
-2
-2.5
-3
log(N) (s-1)
d
10
0
-10
I-<I> (dB)
log(<ε>) (m2 s-3)
-5
-6
-7
-8
e
332.55
332.6
332.65
332.7
time (yearday)

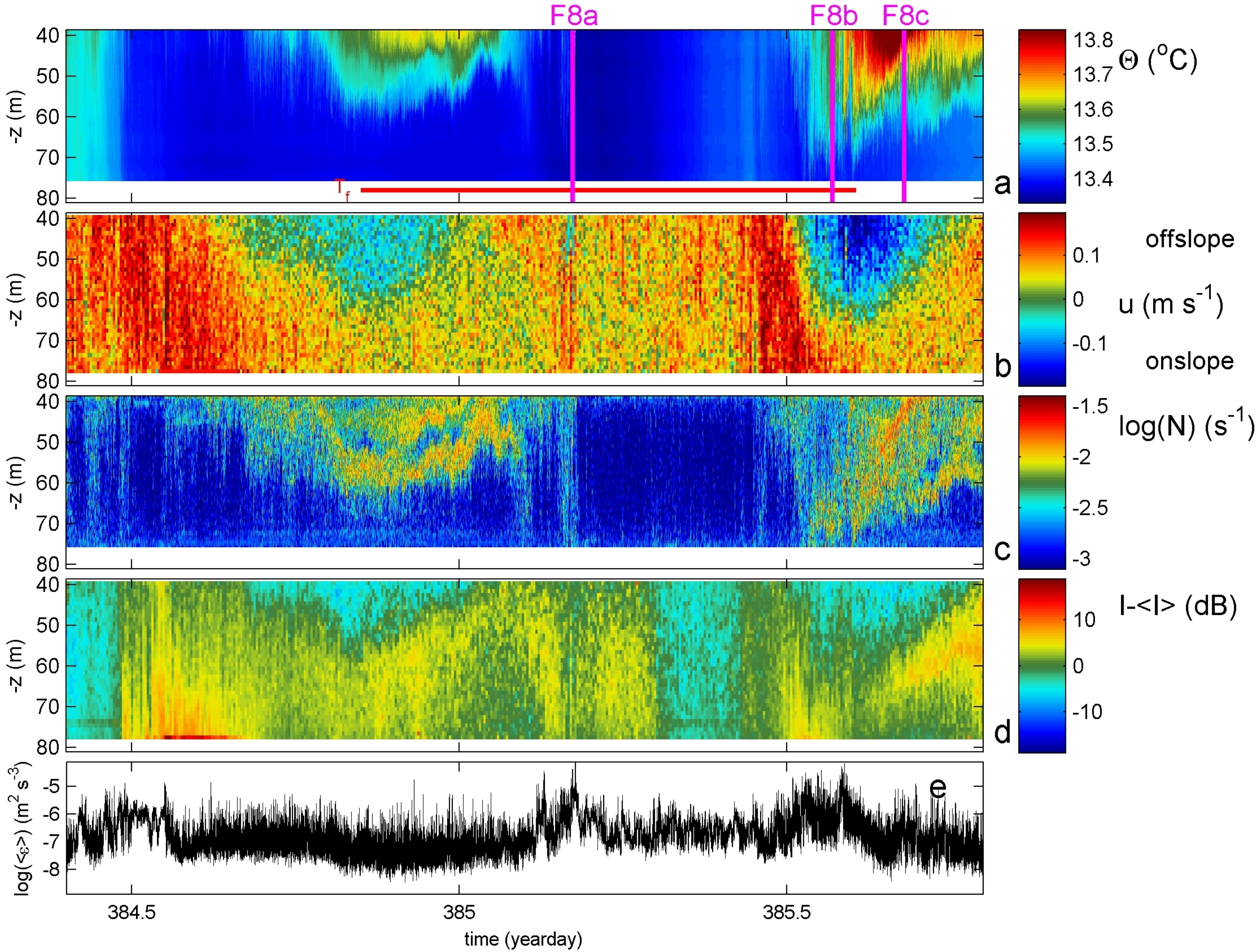

F8a
F8b
F8c
T$_f$
-z (m)
40
50
60
70
80
a
13.8
13.7
13.6
13.5
13.4
Θ (°C)
b
offslope
0.1
0
-0.1
u (m s^{-1})
onslope
c
-1.5
-2
-2.5
-3
log(N) (s^{-1})
d
10
0
-10
I-<I> (dB)
e
log(<ε>) (m^2 s^{-3})
-5
-6
-7
-8
384.5
385
385.5
time (yearday)

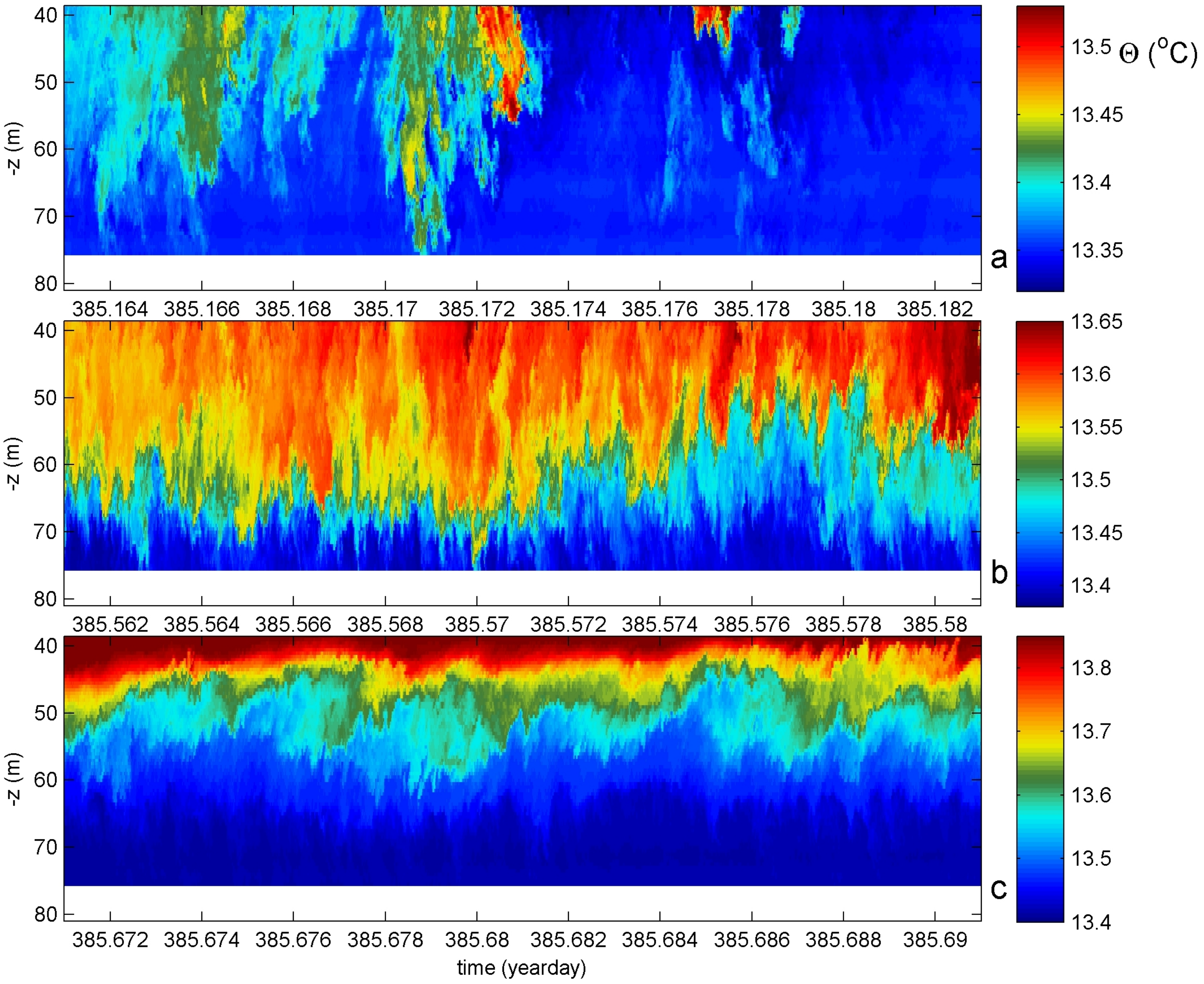

40
50
60
70
80
-z (m)
385.164
385.166
385.168
385.17
385.172
385.174
385.176
385.178
385.18
385.182
a
13.5
13.45
13.4
13.35
Θ (°C)
385.562
385.564
385.566
385.568
385.57
385.572
385.574
385.576
385.578
385.58
b
13.65
13.6
13.55
13.5
13.45
13.4
385.672
385.674
385.676
385.678
385.68
385.682
385.684
385.686
385.688
385.69
c
13.8
13.7
13.6
13.5
13.4
time (yearday)